SCIENCE CHINA
Technological Sciences

Special Topic: Smart and Functional Fiber Materials
•Article•

June 2019 Vol.62 No.6: 971–981
https://doi.org/10.1007/s11431-018-9441-1

Structural characterization of carboxyl cellulose nanofibers extracted from underutilized sources

ZHAN ChengBo[1†], SHARMA Priyanka R.[1†], GENG LiHong[1,2], SHARMA Sunil K.[1], WANG RuiFu[1], JOSHI Ritika[1] & HSIAO Benjamin S.[1*]

[1] *Department of Chemistry, Stony Brook University, Stony Brook NY 11794-3400, USA;*
[2] *National Engineer Research Center of Novel Equipment for Polymer Processing, Key Laboratory of Polymer Processing Engineering of Ministry of Education, South China University of Technology, Guangzhou 510640, China*

Received October 10, 2018; accepted January 10, 2019; published online May 5, 2019

Two different chemical methods, TEMPO-oxidation and nitro-oxidation, were used to extract carboxyl cellulose nanofibers (CNFs) from non-wood biomass sources (i.e., jute, soft and hard spinifex grasses). The combined TEMPO-oxidation and homogenization approach was very efficient to produce CNFs from the cellulose component of biomass; however, the nitro-oxidation method was also found to be effective to extract CNFs directly from raw biomass even without mechanical treatment. The effect of these two methods on the resulting cross-section dimensions of CNFs was investigated by solution small-angle X-ray scattering (SAXS), transmission electron microscopy (TEM) and atomic force microscopy (AFM). The UV-Vis spectroscopic data from 0.1 wt% TEMPO-oxidized nanofiber (TOCNF) and nitro-oxidized nanofiber (NOCNF) suspensions showed that TOCNF had the highest transparency (> 95%) because of better dispersion, resulted from the highest carboxylate content (1.2 mmol/g). The consistent scattering and microscopic results indicated that TOCNFs from jute and spinifex grasses possessed rectangular cross-sections, while NOCNFs exhibited near square cross-sections. This study revealed that different oxidation methods can result in different degrees of biomass exfoliation and different CNF morphology.

cellulose nanofibers, TEMPO-oxidation, nitro-oxidation, SAXS, microscopy, jute, spinifex

Citation: Zhan C B, Sharma P R, Geng L H, et al. Structural characterization of carboxyl cellulose nanofibers extracted from underutilized sources. Sci China Tech Sci, 2019, 62: 971–981, https://doi.org/10.1007/s11431-018-9441-1

1 Introduction

Cellulose is the most abundant, sustainable and renewable natural polymer, and it has been utilized in a myriad of applications since the beginning of human civilization. Nanocellulose, which can be extracted from the cell wall of any plant (wood or non-wood), has drawn a great deal of research interests because of its unique properties, including high surface-to-volume ratio, good mechanical strength, low thermal expansion coefficient, high optical transparency, good gas barrier properties, good chemical resistance, low environment impact and easy functionalizability [1–4]. In specific, nanocellulose has been considered as an effective reinforcing agent to increase the composite properties, such as stiffness, strength, chemical and thermal stabilities [5–9]. These properties also make the nanocellulose-based composite membranes suitable for separation applications [10–16]. For example, nanocellulose has been shown to be a good barrier layer material for ultrafiltration and nanofiltration membranes [17–19]. Nanocellulose has also been demonstrated as an excellent adsorptive material for removal of charged contaminants in molecular or particle forms from water [4,20–23]. The typical methods to remove charged

†These authors contributed equally to this work.
*Corresponding author (email: benjamin.hsiao@stonybrook.edu)

contaminants (e.g., heavy metal ions, small chemicals and viruses) in water purification include sorption, chemical precipitation, membrane separation and electrochemical treatment [24–27], where sorption remains to be the most popular process in low-energy and low-cost operations with activated carbons being the mainstay of adsorptive media [28–31]. It turns out that nanocellulose is a promising alternative to replace activated carbon due to its high adsorptive performance [14,15,32,33], if the material can be prepared from low-valued biomass using low-cost process. Unfortunately, to date, the cost of producing nanocellulose from conventional routes is significantly higher than that of making activated carbon [16,34–37]. Furthermore, there are many other emerging advanced applications of nanocellulose, including fuel cells, solar cells, biomedical devices, gas barrier films, sensors, dispersion stabilizers for carbon nanotubes [38–45].

There are several forms of nanocellulose that can be extracted from biomass. The three most commonly encountered forms are cellulose nanocrystal (CNC) [46,47], cellulose nanofiber (CNF) [20,48,49], and spherical nanoparticle (SNP) [45,50–54]. Recently, the Technical Association of the Pulp and Paper Industry (TAPPI WI3021) has announced new rules to denote the terminology for cellulose nanomaterials based on their properties. Among these, CNC and CNF are the most popular form of nanocellulose. CNC has the highest crystallinity and possesses rod-like morphology with conical tips; it is usually produced by strong acid hydrolysis of cellulose or microcrystalline cellulose (MCC), where the process removes the amorphous regions leaving behind the crystalline form of cellulose [46]. CNF can be prepared by mechanical homogenization, or the combined chemical and mechanical approach. The typical chemical methods include carboxymethylation and carboxylation (e.g. TEMPO-oxidation or recently demonstrated nitro-oxidation) [48,55]. These methods introduce negative charges on the cellulose surface in the form of carboxylate ions, creating electrostatic repulsive forces that facilitate the fibrillation of microscale material into nanocellulose [56]. The subsequent use of mechanical treatment, such as homogenization, can further improve the fibrillation process.

The current chemical methods for nanocellulose extraction are mostly driven by the forest industry, where the structure of wood biomass is dense and compact, or by the cotton industry, where the content of cellulose is extremely high (can be > 90%). In the extract of nanocellulose from wood biomass, the methods usually involving multiple treatment steps, multiple chemical reagents and high electrical energy and water consumption. In addition, the methods often require the use of cellulose with little hemicellulose, lignin and other impurities to be effective. The complex treatment procedures are often not necessary to defibrillate non-wood biomass. In our laboratory, we have demonstrated a simpler nitro-oxidation method, using mainly the mixture of nitric acid and sodium nitrite, that can extract CNFs directly from untreated (raw) non-wood biomass [55]. In this method, the lignin component is depolymerized into soluble benzoquinone products by nitrogen oxide species (produced by the reaction of nitric acid and sodium nitrite), and the hemicellulose component is broken down into xylose and other by-products by nitric acid [55,57]. In addition, the generation of nitroxonium ions can selectively oxidize the primary hydroxyl groups of anhydroglucose units of cellulose to carboxyl groups. As a result, the nitro-oxidation method efficiently reduces the need for multiple chemicals, and the consumption of electric energy and water for producing functional nanocellulose.

In this study, we compare the morphology of CNFs produced from two non-wood biomass species using the popular TEMPO-oxidation method and the simple nitro-oxidation methods. The chosen biomass species were jute fiber, soft and hard spinifex grasses, where both are considered low-valued biomasses today. Jute fiber is abundant in southern Asia including China, and spinifex grass is widely spread in the arid regions of Australia. These biomasses are vastly underutilized when compared to the wood-based biomass. The morphological information (i.e. cross-section dimensions) of the resulting TEMPO-oxidized cellulose nanofibers (TOCNF) and nitro-oxidized cellulose nanofibers (NOCNF) were characterized by solution small-angle X-ray scattering (SAXS), transmission electron microscopy (TEM) and atomic force microscopy (AFM) techniques. The results have allowed us to develop new insight into the structure and processing relationship using different chemical methods, where this knowledge will be useful for us to consider other underutilized biomasses, such as agriculture waste and invasive species, as resources to generate new, efficient and low-cost water purification materials (e.g., flocculants, adsorbents, and membrane filters).

2 Experiment

2.1 Materials

Untreated (raw) jute fibers were provided by Toptran Bangladesh Ltd. (Bangladesh). Soft spinifex (*Triodia pungens*, abbreviated as SS) and hard spinifex (*Triodia longiceps*, abbreviated as HS) samples were kindly provided by Professor Darren Martin's group at the University of Queensland. Sodium chlorite ($NaClO_2$), 2,2,6,6-tetramethyl-1-piperidinyloxy (TEMPO), sodium hypochlorite solution (NaClO, available chlorine 10%–15%), sodium bromide (NaBr) sodium hydroxide (NaOH), nitric acid (ACS reagent, 65%–70%) and sodium nitrite (ACS reagent ≥97%), were purchased from Sigma-Aldrich and used without further purification.

2.2 Pretreatment of biomass samples for TEMPO-oxidation

Dried raw jute fibers were cut into small pieces with length ≤ 5 mm, which were then immersed in NaOH solution (1 mol/L) for preliminary delignification. The mixture was kept stirring for 24 h at room temperature. Subsequently, the upper liquid was decanted off to separate the delignified fibers. The recovered fibers were rinsed by deionized water (DI water) for 3 times and dried in an oven at 80°C for 24 h. The dried delignified fibers were bleached using acidic $NaClO_2$ solution (1% w/v, where the pH was stabilized around 5 by acetic acid and sodium acetate buffer) at 70°C for 2 h. The bleaching steps were repeated for 5 times. The resulting fibers (in white color) were then rinsed by DI water, dried and stored before use.

Pretreatment of spinifex fibers were carried out according to the method mentioned in ref. [58]. In brief, spinifex fibers with an average length ≤10 mm were delignified at 80°C for 2 h using sodium hydroxide solution (0.5 mol/L) with a 10:1 solvent to sample ratio. The treated fibers were washed with DI water and dried in oven at 80°C for 24 h. The delignified fibers were bleached 2 times using an acidic solution of sodium chlorite (1% w/v, the pH was decreased around 4 by glacial acetic acid) having a 30:1 solvent to sample ratio at 70°C for 1 h. The recovered fibers were subsequently rinsed by DI water, dried and stored before use.

2.3 Preparation of TOCNF suspensions

TEMPO-oxidation to extract CNFs from different delignified biomass samples (jute, hard spinifex or soft spinifex) was carried out using the procedure published in ref. [59]. In brief, 10 g (or 61.7 mmol) of biomass was suspended in 960 mL of DI water, where the mixture were subsequently added with 1 g (9.72 mmol) of NaBr and 0.1 g (0.64 mmol) of TEMPO agent. The mixture was stirred for 15 min to dissolve the TEMPO agent, whereby 75 g (121 mmol) of 12% NaClO aqueous solution was added. During the reaction, the pH of the suspension was monitored and maintained between 10 and 10.5 using NaOH solution (0.1 mol/L). After being stirred at room temperature for 24 h, the reaction was terminated by addition of 2 mL ethanol. The oxidized fiber slurry was then dialyzed (using a dialysis bag, Spectral/Por, with MWCO: 6–8 kDa) against DI water until the conductivity of the dialysate was below 5 μS (after equilibration for 12 h). Finally, the slurry was mechanically treated using a sonication homogenizer (Cole Parmer, VCX-400) operated at a power of 320 W for 3 min (in ice bath). Large and unreacted fibers were removed by centrifuging the suspension at 4700×*g* for 10 min. The supernatant was then collected and measured with a total organic carbon analyzer (TOC, TOC-5000, Shimadzu Corp., Japan) to determine the concentration, where the stock suspension was then diluted into the desired concentration for further study.

2.4 Preparation of NOCNF suspensions

NOCNFs were extracted directly from untreated biomass samples using the nitro-oxidation method [55]. In this preparation, 5 g of finely cut raw biomass sample (jute fibers, hard spinifex and soft spinifex) was placed in a three-neck round-bottom flask, where 70 mL (22.2 mmol) of nitric acid (65%–70%) was subsequently added. After 15–20 min of immersion, when the sample became completely wet, 9.80 g (28 mmol) of sodium nitrite was added into the flask. Upon addition of sodium nitrite, intense red fumes were formed inside the flask. To prevent the red fumes from escaping, mouths of the round flask were covered with stoppers and the flask was maintained at 50°C for 12 h. The reaction was then quenched by addition of 500 mL distilled water. After equilibration, the liquid supernatant (upper layer), containing the unreacted acid and reagents were removed by decantation. Distilled water was added to the residual white fibers, where the mixtures were stirred, settled and decanted again to remove the supernatant. The above procedure was repeated 2–3 times until the fibers started to suspend in water. The suspension was diluted with water and centrifuged at 5000×*g* for 10 min, and the supernatant was removed. This step was repeated 1–2 times until the pH of the supernatant reached above 2.5. The suspension was then dialyzed (using a dialysis bag Spectral/Por, MWCO: 6–8 kD) and equilibrated for 6–8 d until the conductivity of water reached below 5 μS. The resulting suspension contained CNFs with COOH groups and the corresponding pH was between 2.8–3.0. To improve dispersion of the fibers, the suspension was treated with 4 wt% of sodium bicarbonate (1:10 wt/v%) until the pH reached 7.5 to obtain carboxylate groups ($-COO^-$) having ionic charges.

2.5 Characterization

Ultraviolet-visible light spectroscopy (UV-Vis). The UV-Vis measurement was performed by a ThermoFisher GEN10S UV-Vis Spectrometer. In the typical experiment, 1 mL of the TOCNF or NOCNF suspension was placed in a fishier semi-micro quartz cuvette having 1 cm path length. The range of chosen wavelength was set from 400 to 800 nm with an interval of 0.5 nm for measurement.

Transmission electron microscopy (TEM). The TOCNF or NOCNF suspension (2 μL) at a concentration of 0.1 wt% was cast on a glow-discharged carbon film coated copper grid (300 mesh). The suspension was allowed to stay on the grid for about 1 min, where the excess liquid was drawn off the grid using a filter paper. The cast sample was then stained by depositing a uranyl acetate solution (1.0 wt%, 1.5 μL) on

the grid. The staining solution was allowed to enhance the contrast of the sample for about 30 s before removal using a filter paper. The stained sample was left in the air for 5 min. The TEM observation was performed at the Center for Functional Nanomaterials (CFN) in Brookhaven National Laboratory (BNL) using a JEOL JEM-1400 microscope (JEOL, Tokyo, Japan) equipped with a CCD camera (ORIUS SC200, Gatan, Inc., USA) operated at 120 kV. The TEM image analysis was performed using the ImageJ software.

Atomic force microscopy (AFM). The AFM measurement was performed in the tapping mode using a Bruker Dimension ICON scanning probe microscope (Bruker Corporation, USA) equipped with a Bruker OTESPA tip (the radius was around 7 nm) at the Advanced Energy Research and Technology Center (AERTC) in Stony Brook University. In sample preparation, a Piranha cleaned silica wafer substrate was used to support the TOCNF or NOCNF sample, where the corresponding suspension (0.0015 wt%) was deposited on the substrate and dried overnight. The AFM image analysis was carried out by the NanoScope Analysis software provided by Bruker.

Solution small-angle X-ray scattering (SAXS). Solution SAXS measurements of TOCNF or NOCNF suspensions at different concentrations were carried out at the LiX Beamline in the National Synchrotron Light Source II (NSLS-II) at BNL. During the measurement, 40 μL of suspension was sucked into the sample stage, which contained a long slit (diameter of 1 mm) sealed by mica to form a capillary geometry. To minimize the radiation damage, the suspension was driven back and forth continuously through the capillary using a syringe pump during measurement. The chosen X-ray wavelength was 1.14 Å. The SAXS data were collected by a PILATUS R 1M detector with the sample-to-detector distance of 3.62 m. Two PILATUS R 300K detectors covering the wide-angle range were utilized to collect the wide-angle X-ray scattering (WAXS) data, where the sample-to-detector distances were 0.308 and 1.20 m, respectively. A silver behenate standard was used to calibrate the scattering angle. To correct the background scattering, the measurement of a buffer solution (i.e., water) was carried out after measurements of every 3 samples. For each measurement, five 3-second scans were taken and averaged before the removal of any outlier data. The data processing was carried out using an IPython-based software package developed at the LiX beamline. In this analysis, raw 2D images were converted into linear scattering profiles after masking dead pixels and beam-stop pixels. The SAXS and WAXS data were merged together, and the background scattering (from the buffer) was subsequently subtracted to produce the excess scattering profile for the suspension. In this study, only the profile in the small-angle region (dominated by the CNF cross-section dimensions) was fitted using a ribbon model, where the fitting was accomplished by the SASView software package developed at the National Institute of Standards and Technology (NIST) Center for Neutron Research (NCNR).

3 Results and discussion

3.1 TEMPO-oxidation of jute, soft spinifex and hard spinifex

During typical pulping process, biomass is always cut into small pieces to improve the alkalization and bleaching efficiency. The bleaching pretreatment was also adopted here for the TEMPO-oxidation treatment. The original jute samples were in the rope-like form of long fibers, and they were cut into small pieces with an average length $\leq$ 5 cm. The spinifex samples (soft and hard spinifex) were provided as short fibers with an average length $\leq$ 10 mm, and they were used without further cutting (the images of raw biomass and their pulp fibers are shown in Figure 1). After the TEMPO-oxidation treatment, the cellulose microfiber suspension was further defibrillated in a homogenizer, followed by centrifugation to remove the big and unreacted pieces. A photograph of the resulting TOCNF suspensions is also shown in Figure 1.

It is known that both TEMPO-oxidation and nitro-oxidation methods can introduce carboxylate groups (-COO^-) onto the cellulose surface, where these negatively charged groups would create electrostatic repulsion forces to facilitate the defibrillation process [48,55,60]. When fully defibrillated, the resulting cellulose nanofibers should have cross-sectional dimensions (width and thickness) well below the wavelength of light (300–700 nm), but their lengths, or the corresponding fibrous colloidal size, could be within the range of the wavelength, depending on the processing conditions. The suspension can generate high transparency in the UV-Vis measurement, if the colloidal size is larger or smaller than the wavelength of light; or lower transparency, if the colloidal size is in the same range of the wavelength. In Figure 1, it was seen that both soft spinifex TOCNF and jute TOCNF suspensions (all at 0.1 wt% concentration) exhibited approximately the same transmittance (91%), whereas the hard spinifex TOCNF suspension showed lower transmittance (less than 90%). This may be due to the following reasons. It is known that TEMPO-oxidation is a mild oxidation treatment, where the resulting fiber length can be quite long (>1 μm). When the fiber "particle" is extended, the colloidal size can be above the light wavelength and cause little or no interference with light (i.e., higher transparency). However, when the fiber particle collapses, the smaller colloidal size can interfere with light and reduce the transmittance.

The expansion and contraction behavior of the fibrous colloidal particle may be directly related to the charge density on the fiber surface. To test this hypothesis, the degree of oxidation of varying TOCNF was determined by the con-

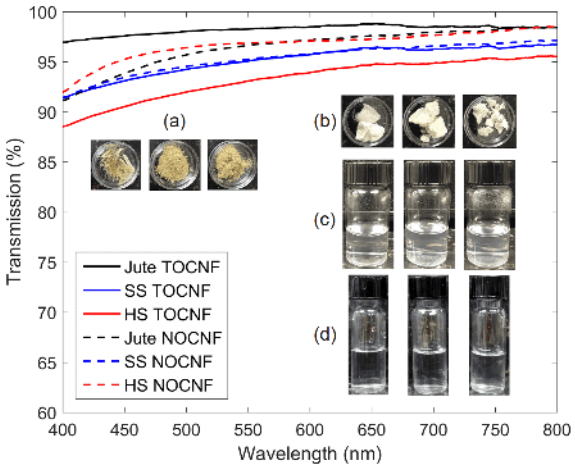

Figure 1 (Color online) The UV-Vis spectra of TOCNF and NOCNF suspensions (0.1 wt%) from jute, soft spinifex (SS), and hard spinifex (HS). Photos of the biomass and the nanocellulose suspensions are listed on the bottom right corner. (a) From left to right, the raw biomass samples of jute, soft spinifex and hard spinifex; (b) from left to right, the pulp of jute, soft spinifex and hard spinifex; (c) from left to right, the 0.1 wt% TOCNF suspensions of jute, soft spinifex and hard spinifex; (d) from left to right, the 0.1 wt% NOCNF suspensions of jute, soft spinifex and hard spinifex.

ductometric titration method. The results showed that the carboxylate content for jute, soft spinifex, and hard spinifex TOCNF suspensions were 1.2, 1.0 and 0.62 mmol/g, respectively. These results are reasonable, as we argue that higher carboxyl content give rise to stronger repulsion forces within the CNF particulates leading to larger colloidal size, and thus less interactions with the visible light. However, we note that the efficiency variation of the chosen TEMPO-oxidation method to treat different biomass must also play a role. In the three chosen biomass samples, the content of hemicellulose in raw spinifex is very high [58] (with hard spinifex being the highest) and that of jute is the lowest. As a result, the same ordering probably also persists after bleaching. In the typical cell wall structure in plant, hemicellulose macromolecules tether the cellulose microfibrils together and form nanofibers, where lignin and hemicellulose macromolecules further bind the nanofibers together and form macrofibers. It has been reported that, after the pulping process, the higher content of hemicellulose (also behaves as a "lubricant" between cellulose nanofibers) and the lower content of lignin (as in the spinifex grass) could greatly reduce the energy consumption in the production of mechanically fibrillated nanocellulose [58]. The presence of hemicellulose might inhibit the efficiency of TEMPO-oxidation in fabricating CNF. This is because the TEMPO reaction is effective in the oxidation of primary hydroxyl groups in cellulose, where these functional groups are also present in hemicellulose [61,62]. Hence, the TEMPO reaction may be less effective in the sample having higher hemicellulose content, where the presence of unreacted hemicellulose could further cause the formation of aggregates and lower the transmission of the TOCNF suspension.

3.2 Nitro-oxidation of jute, soft spinifex and hard spinifex

Nitro-oxidation was performed on raw jute, hard spinifex and soft spinifex biomass without having any pretreatment. The photos of the final NOCNF suspensions (0.1 wt%) are shown in Figure 1(d). These suspensions were all very clear and exhibited high transparency above 91%. Interestingly, the hard spinifex NOCNF showed higher transparency (92%) than the hard spinifex TOCNF. This might be because the use of nitric acid broke down the hemicellulose component, which subsequently dissolved in water, in the nitro-oxidation treatment. Thus, this would result in the lower hemicellulose content in the NOCNF suspension than that in the TOCNF suspension. Again, we argue that the presence of hemicellulose might result in higher aggregation tendency.

The carboxylate content of NOCNF produced from the chosen biomass samples were also determined by the conductometric titration method [63]. The results indicated that the carboxylate contents of NOCNF of jute fibers, soft spinifex and hard spinifex samples prepared by the nitro-oxidation method were 1.06, 0.18 and 0.16 mmol/g, respectively. The lower carboxylate content in hard and soft spinifex as compared to jute fibers under the same reaction condition is most probably due to the presence of high hemicellulose content in spinifex [64]. It is conceivable that, the active oxidizing specie in nitric acid oxidation-nitroxonium ions (NO^+) may have reacted preferentially to hemicellulose moiety rather than cellulose moiety in spinifex. As the oxidized products of hemicellulose are water soluble [65], the carboxylate content measured reflects the surface property on the NOCNF only. As a result, the higher hemicellulose content can lead to lower carboxylate content measured. This is consistent with the observation that the carboxylate content values were relatively lower in NOCNF than those in TOCNF as the nitro-oxidation was performed on raw untreated samples while TEMPO-oxidation was performed on the cellulose component.

3.3 Characterization of TOCNF and NOCNF by microscopic techniques

Microscopic techniques can provide very useful information to understand the structure of the material in micro- and nano-scale. The visualization of the objects can lead to direct analysis of the morphological parameters. In the case of CNF, the techniques are particularly useful to determine the cross-sectional dimensions of the nanofibers, which can be correlated to the average pore size of the non-woven membrane. For example, when TOCNF was used to produce the

barrier layer of the thin-film composite (TFC) membrane, the mean cross-sectional dimension of the membrane was found to linearly correlate with both mean pore size and maximum pore size of the membrane, thus the rejection performance [66]. However, different microscopic techniques seem to have different limitations in determining the proper cross-sectional dimensions.

For example, Figure 2 illustrates the AFM images of TOCNF and NOCNF samples extracted from jute, soft spinifex, and hard spinifex. From these images, both height and width information can be extracted. In AFM images of TOCNF, white spots with high brightness were observed. These spots were probably due to the stacking of multiple fibers or contamination of dust particles, and thus were carefully avoided for analysis. In each AFM image, three regions containing a single nanofiber were analyzed, where the corresponding height and width profiles are illustrated below the AFM image (Figure 2). From these profiles, the nanofiber width (around 4 nm, will be discussed later) could not be easily determined as it is smaller than the radius of the AFM tip (around 7 nm). However, the nanofiber thickness was estimated from the maximum height value, where the average thickness was 1.5, 1.4 and 1.7 nm for jute TOCNF, soft spinifex TOCNF, and hard spinifex TOCNF, respectively. In contrast, the average thicknesses for NOCNF samples were found to be larger, they were 3.1 nm for jute, 3.8 nm for soft spinifex, and 4.5 nm for hard spinifex. The average nanofiber thickness values determined from the height profile for different biomass samples are summarized in Table 1, and they are consistent with the results from solution SAXS analysis in the next section.

The AFM images also illustrated the morphology and aggregation behavior of the CNFs investigated. The results are shown in Figure 3, where the AFM images were acquired at a lower magnification. In Figure 3(a)–(c), it was found that TOCNF from jute, soft and hard spinifex samples all exhibited typical fibrous morphology, but they possessed different aggregation tendency. Jute TOCNF appeared to be well dispersed; soft spinifex TOCNF was found to have aggregation tendency, while single nanofibers were still discernible; hard spinifex TOCNF exhibited the greatest tendency to aggregate and self-assembled into stacks. The existence of the agglomerated structures in soft and hard TOCNF samples, which were also confirmed by solution SAXS experiments (in the next section), agreed well with the optical transparency and the degree of oxidation results of the TOCNF suspensions. In Figure 3(d)–(e), all NOCNF samples exhibited the shape of short filament, similar to that of CNC. Jute and soft spinifex NOCNF exhibited good dispersion, while hard spinifex NOCNF appeared to have greater aggregation tendency. This was also consistent with the degree of oxidation results. The difference in morphology (e.g. TOCNF possessed much longer fiber lengths than

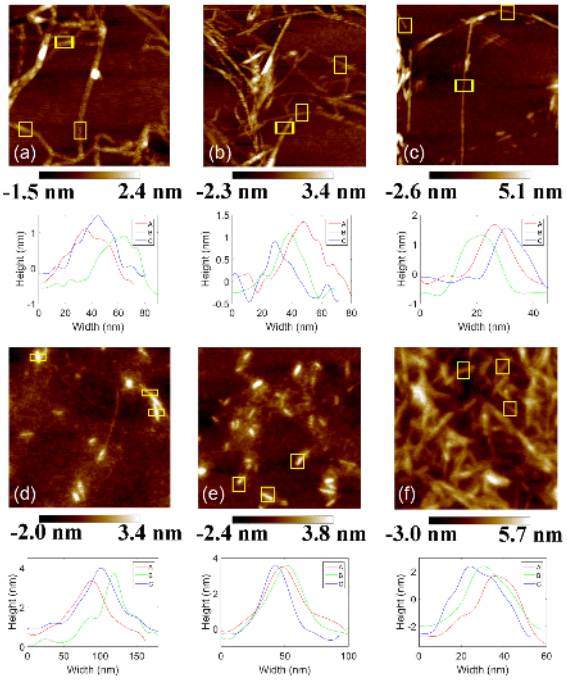

Figure 2 (Color online) AFM images of TOCNF and NOCNF suspensions of jute, soft spinifex and hard spinifex with concentration of 0.0015wt%. The region for each image was 1 μm×1 μm. The height distribution profiles of three selected sections of each sample (labeled by yellow rectangles) are shown underneath the image (the legends A, B and C represent the yellow rectangles from left to right). Upper row: (a) jute TOCNF suspension, (b) soft spinifex TOCNF, (c) hard spinifex TOCNF; bottom row: (d) jute NOCNF suspension, (e) soft spinifex NOCNF and (f) hard spinifex NOCNF.

NOCNF) was resulted from the different processing conditions. It is well known that TEMPO-mediated oxidation is a mild reaction that often retains the long fiber length, while nitro-oxidation comprises the use of strong nitric acid that can remove the hemicellulose and lignin components from raw biomass, but they also inevitably decrease some regions of cellulose and leading to short fiber length.

The width of the CNF can be determined quite precisely by the TEM technique. Figure 4 illustrates the TEM images of jute, soft spinifex and hard spinifex TOCNF and NOCNF samples. The mean width for each sample was determined from the average of the width values of 100–200 fibers from several images and the histograms are shown in Figure S1 (Supporting Information). All CNF samples exhibited a Gaussian-like distribution in width and the average value was in the range of 4–6 nm. The width results from different samples are also summarized in Table 1, which was further confirmed by the solution SAXS technique. We note that TEM cannot easily determine the thickness of the nanofiber, as which is ribbon-like. Thus after the sample preparation, the nanofibers mostly lay flat, instead of standing on their edges, on the TEM grid. Clearly, the flat orientation gives rise to higher van der Waal interacting forces and is more favorable. In Figure 4, it was also apparent that TOCNF

Table 1 Height and width information measured by microscopy (AFM and TEM) and solution SAXS. The average and deviation for solution SAXS were extracted from the fitting results. The statistical average and deviation for microscopic data were calculated based on the image analysis

Nanocellulose	Height (nm)		Width (nm)	
	AFM	Solution SAXS	TEM	Solution SAXS
Jute TOCNF	1.5 ± 0.1	1.4 ± 0.7	4.0 ± 0.8	4.7 ± 1.5
Soft spinifex TOCNF	1.5 ± 0.1	1.5 ± 0.8	4.2 ± 0.9	6.2 ± 2.4
Hard spinifex TOCNF	1.8 ± 0.1	1.6 ± 0.8	4.4 ± 1.0	6.6 ± 2.5
Jute NOCNF	3.0 ± 0.3	3.2 ± 2.2	5.6 ± 1.5	7.1 ± 3.7
Soft spinifex NOCNF	3.9 ± 0.2	3.9 ± 2.6	5.2 ± 1.3	6.5 ± 3.5
Hard spinifex NOCNF	4.6 ± 0.2	4.7 ± 2.3	5.6 ± 1.6	7.0 ± 2.4

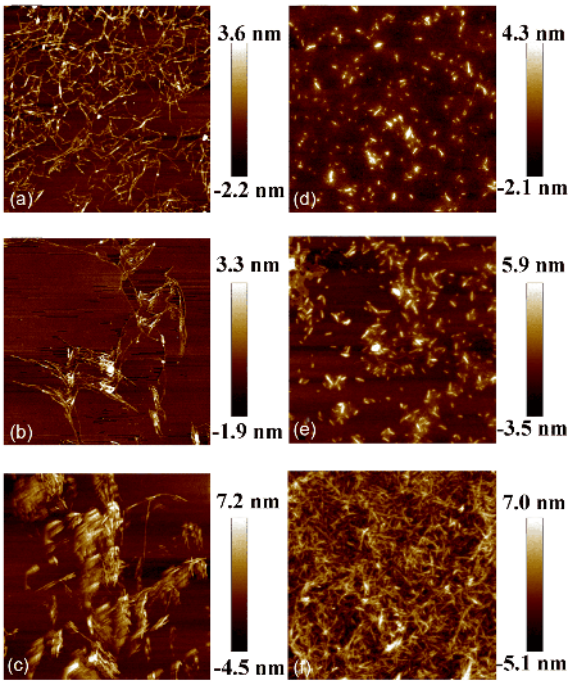

Figure 3 (Color online) Left column: AFM images of TOCNF suspensions of (a) jute, (b) soft spinifex and (c) hard spinifex. Right column: AFM images of NOCNF suspensions of (d) jute, (e) soft spinifex and (f) hard spinifex. The images were acquired with 0.0015 wt% suspensions and the chosen image size was 5 μm× 5 μm.

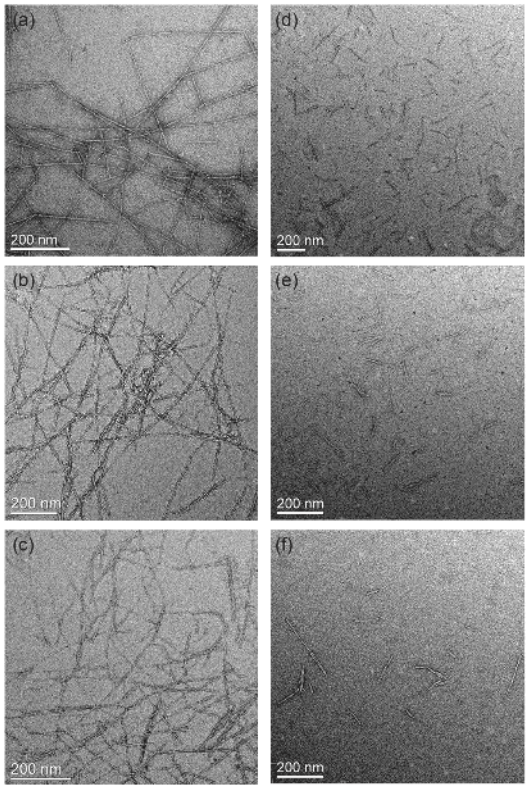

Figure 4 TEM images for TOCNF and NOCNF samples. Left column: TOCNF prepared from (a) jute, (b) soft spinifex, and (c) hard spinifex. Right column: NOCNF prepared from (d) jute, (e) soft spinifex and (f) hard spinifex.

possessed a long fiber length and NOCNF exhibited a much shorter length. This result was consistent the AFM observation. Without question, TEM and AFM are complementary techniques for characterization of the cross-sectional dimensions of cellulose nanofibers that have either a rectangular or near square shape [67]. In short TEM is particularly useful for determining the width of the nanofiber and AFM is very useful for determining the thickness of the nanofiber. Both techniques can provide overall morphological and aggregation information.

3.4 Characterization of TOCNF and NOCNF suspensions by solution SAXS

Microscopic techniques allow direct visualization of the object virtually down to nanoscale size, but they often encounter experimental challenges with the sample preparation and the area of investigation. When the fraction of sample under observation becomes so small such that it is difficult to get a good statistical analysis of the sample in general. In this perspective, the solution small-angle X-ray scattering (SAXS) technique can resolve the above issues. The sample preparation for solution SAXS is very straightforward. It requires a relatively small volume (1000 μL) of solution sample when synchrotron X-ray is used, where the preparation scheme does not need to be carried out in a dust-free environment (as for solution light scattering). Additionally, all CNFs in the irradiated volume can be detected in the

scattering profile, providing good statistical information by the data analysis. Therefore, microscopic and scattering tools often compensate each other and the characterizations from both techniques are necessary to paint a detailed view of the structure and morphology.

It has been clearly demonstrated that the cross-sectional parameters (i.e., width and thickness, both in the range of a few nanometers) dominate the scattering signals in the typical SAXS detection range [68]. The ribbon shape or the rectangular shape for the cross-section of the nanofiber is certainly consistent with the crystallographic packing of cellulose chains in the unit cell [69]. In this study, the solution SAXS data were analyzed using the polydisperse-ribbon model, which is a simplified parallelepiped model having the analytical form. Based on this model, the corresponding 1D scattered intensity in the mid-q range can be expressed as follows [70]:

$$\frac{I(q)}{c}=\frac{2\pi}{q^3}\left\{1-\mathrm{Re}\left[\left(1+\frac{iq\sigma_a^2}{a_0}\right)^{-(a_0/\sigma_a)^2}\right]\right\}\left(b_0^2+\sigma_b^2\right)\times{}_3F_2\left(\frac{1}{2},1+\frac{b_0^2}{2\sigma_b^2},\frac{3}{2}+\frac{b_0^2}{\sigma_b^2};\frac{3}{2},2;-\frac{q^2\sigma_b^4}{b_0^2}\right),$$

where $I(q)$ represents the scattered intensity; a_0 and a_0+b_0 represent the thickness and width of the cross-section, respectively; σ_a and σ_b correspond to the standard deviations for a_0 and b_0, respectively; ${}_3F_2$ is the hypergeometric function; and Re refers to the real part of the term in the brackets. The model fitting was carried out by using a customized plug-in in the SasView software, where the results are listed in Figure 5 and Table 1.

In Figure 5, it was seen that the polydisperse-ribbon model could well describe the scattering profile for both TOCNF and NOCNF suspensions in the mid-q range. However, in spinifex TOCNF and NOCNF suspensions, the fit deviated from the experimental data at the low-q range (the slopes of the experimental curves were higher than those of the fitting curves, as seen in Figure 5(b)). The cause for this deviation can be explained by the presence of larger structures probably from aggregated nanofibers. This behavior was consistent with the results from UV-Vis spectra and AFM images, where the high hemicellulose content in spinifex grass might be responsible for the aggregation behavior.

In Table 1, the cross-sectional dimensions (nanofiber width and thickness) extracted from the solution SAXS data were found that be generally consistent with those determined from the microscopic analysis (TEM-nanofiber width and AFM-nanofiber thickness). It was found that the thicknesses of both TOCNF and NOCNF measured from AFM were very close to those from the solution SAXS measurements, but the widths measured from solution SAXS were notably larger than those from the TEM measurements. The difference in the width measurements can be explained as follows. The solution SAXS results are probably closer to the true width values of the different nanofibers, as they are in the disperse state in water. The TEM results may consist of artifacts resulting from the sample preparation. In the chosen TEM sample preparation scheme, the specimen was prepared by depositing 10 μL of 0.01 wt% suspension on the copper grid, which was dried in air before observation. It is conceivable that the drying process might have causes the nanofiber width to contract slightly. Overall, the solution SAXS, TEM and AFM showed a very good agreement in determining the cross-sectional dimensions of the resulting CNFs.

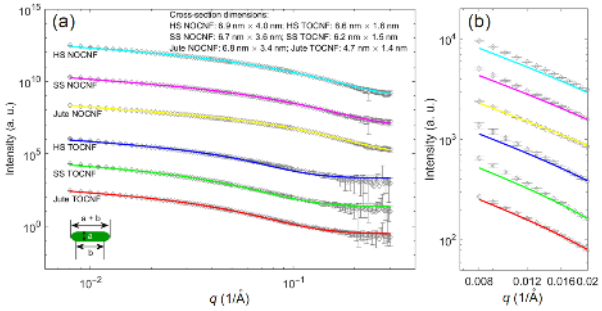

Figure 5 (Color online) (a) The fitting results using the polydisperse ribbon model and the solution SAXS experimental profile for TOCNF and NOCNF suspensions of jute, soft spinifex (SS) and hard spinifex (HS) at the concentration of 0.2 wt%; and (b) the scattering curves and fits in the low-q region. For better clarity, the curves were manually shifted in the vertical direction for both figures. The bottom left diagram exhibits the shape and the parameters of ribbon model, and the fitting results (height, a; width, $a+b$) are listed on the top right corner.

It was very interesting to found that the cross-section of TOCNF samples exhibited a ribbon shape with the width-to-thickness ratio larger than 1, whereas that of NOCNF samples displayed a near square shape with the width-to-thickness ratio close to 1. This difference is explained as follows.

3.5 Morphology difference between TOCNF and NOCNF

It is known that cellulose microfibrils (the smallest building block of cell wall) and nanofibers are tethered by hemicellulose chains in the cell wall of a plant. Furthermore, some hemicellulose chains are also woven into the ordered cellulose microfibrils [71]. Clearly, different oxidation methods can lead to different degree of exfoliation in the cell wall, and thus impact the final nanofiber morphology.

In delignified cellulose biomass, the TEMPO-oxidation process can degrade hemicellulose chains, where the by-products are dissolved by the reaction system [72,73]. This process would provide channels for the oxidants to further penetrate into the cellulose assembly, leading to the oxidation of some inner molecules and a high degree of oxidation. If the process continues, eventually, the glucan chain sheets

(i.e., the $(1\bar{1}0)$ plane for I_β cellulose crystals) can be delaminated, resulting in the creation of two-dimensional cellulose nanostrips containing single layer of cellulose molecules [63]. However, in the chosen oxidation conditions, the oxidation probably occurred mostly on the surface of cellulose nanofibers and only partially inside of the microfibril, where the delamination process due to electrostatic repulsion results in a ribbon like structure.

In nitro-oxidation process, the presence of concentrated nitric acid (65%–70%) can dissolve some low molar mass lignin components and break down the hemicellulose component into xylose and other by-products [65]. The generation of nitrogen oxide species (produced by the addition of nitric acid and sodium nitrite) can further depolymerize the lignin component of the raw biomass by converting the syringyl units on lignin into soluble benzoquinone products [74]. In these nitrogen oxide species, the creation of nitroxonium ions (an active oxidizing specie) can also selectively oxidize the primary hydroxyl groups of anhydroglucose units of cellulose to carboxyl groups leading to the fibrillation of the cellulose component and generation of nanofibers. It appears that the chosen nitro-oxidation conditions created a shorter nanofiber length, and a larger nanofiber thickness. In a recent publication by our group, we demonstrated that the reduced nitric acid concentration (60%) could produce a longer nanofiber length where the optimized oxidation conditions could also reduce the nanofiber thickness [75].

4 Conclusions

In this study, TEMPO-oxidized cellulose nanofibers and nitro-oxidized cellulose nanofibers were extracted from jute, soft spinifex and hard spinifex. TEMPO-oxidation was performed on delignified jute, soft spinifex and hard spinifex fibers. However, the nitro-oxidation was performed on the untreated (raw) jute, hard spinifex and soft spinifex samples. Notably, the mechanical treatment was not performed during the preparation of NOCNF. Both oxidation methods are effective to create cellulose nanofibers containing negatively charged carboxylate groups, which are essential to provide good dispersion in water and high transparency. High resolution microscopic (AFM and TEM) and solution SAXS tools were utilized to characterize the cross-sectional dimensions of TOCNF and NOCNF, and the results were in good agreement with each other. It is found that with the chosen oxidation conditions, the cross-section of TOCNF is ribbon like (or rectangular like), where NOCNF is nearly square like. In addition, the UV-Vis spectroscopy measurement showed that the jute TOCNF suspension had the highest transparency, whereas the hard spinifex TOCNF suspension had the lowest transparency. In the solution SAXS analysis, there was a deviation between the fit and the experimental data in the low-q region for hard and soft spinifex TOCNFs, which was probably due to the aggregation in spinifex TOCNF. Similarly, this aggregation tendency was also visible in AFM measurements. The AFM image of NOCNF of hard spinifex also showed aggregation, consistent to the SAXS data. The atypical behavior of spinifex may be resulted from their high hemicellulose content.

This study clearly shows that the different oxidation pathways and conditions can lead to different degree of exfoliation thus different cross-sectional dimensions and length of the resulting nanofibers, as well as different degree of oxidation. The simplicity of the nitro-oxidation method may be very useful to extract nanocellulose from locally abundant plants with tremendous energy, chemical and water saving benefits.

This work was supported by the Polymer Program from Division of Materials Science of the National Science Foundation of USA (Grant No. DMR-1808690). The authors thank Professor Darren Martin group at University of Queensland for providing the raw materials and helpful discussions. The authors also thank Dr. YANG Lin and Dr. CHODANKAR Shirish at the LiX beamline, which operates under a DOE BER contract DE-SC0012704 and is supported by an NIH-NIGMS (Grant No. P41GM111244). This research used electron microscopy resources of the Center for Functional Nanomaterials, which is a U.S. DOE Office of Science Facility. The facilities at Brookhaven National Laboratory operate under Contract No. DE-SC0012704. We also thank Dr. CHANG Chung-Chueh at AERTC for his assistance of the AFM measurement.

Supporting Information

The supporting information is available online at tech.scichina.com and link.springer.com. The supporting materials are published as submitted, without typesetting or editing. The responsibility for scientific accuracy and content remains entirely with the authors.

1 Dufresne A. Nanocellulose: A new ageless bionanomaterial. Mater Today, 2013, 16: 220–227
2 Wang H, Li D, Zhang R. Preparation of ultralong cellulose nanofibers and optically transparent nanopapers derived from waste corrugated paper pulp. BioResources, 2013, 8: 1374–1384
3 Moon R J, Martini A, Nairn J, et al. Cellulose nanomaterials review: Structure, properties and nanocomposites. Chem Soc Rev, 2011, 40: 3941–3994
4 Sharma P R, Chattopadhyay A, Sharma S K, et al. Efficient removal of UO_2^{2+} from water using carboxycellulose nanofibers prepared by the nitro-oxidation method. Ind Eng Chem Res, 2017, 56: 13885–13893
5 Siqueira G, Bras J, Dufresne A. Cellulosic bionanocomposites: A review of preparation, properties and applications. Polymers, 2010, 2: 728–765
6 Hubbe M A, Rojas O J, Lucia L A, et al. Cellulosic nanocomposites: A review. BioResources, 2008, 3: 929–980
7 Siró I, Plackett D. Microfibrillated cellulose and new nanocomposite materials: A review. Cellulose, 2010, 17: 459–494
8 Lalia B S, Samad Y A, Hashaikeh R. Nanocrystalline-cellulose-reinforced poly(vinylidenefluoride-*co*-hexafluoropropylene) nanocomposite films as a separator for lithium ion batteries. J Appl Polym Sci, 2012, 126: E442–E448
9 Emami Z, Meng Q, Pircheraghi G, et al. Use of surfactants in cellulose nanowhisker/epoxy nanocomposites: Effect on filler dispersion and system properties. Cellulose, 2015, 22: 3161–3176

10 Razaq A, Nyström G, Strømme M, et al. High-capacity conductive nanocellulose paper sheets for electrochemically controlled extraction of DNA oligomers. PLoS ONE, 2011, 6: e29243
11 Ma H, Burger C, Hsiao B S, et al. Nanofibrous microfiltration membrane based on cellulose nanowhiskers. Biomacromolecules, 2012, 13: 180–186
12 Wang R, Guan S, Sato A, et al. Nanofibrous microfiltration membranes capable of removing bacteria, viruses and heavy metal ions. J Membrane Sci, 2013, 446: 376–382
13 Ferraz N, Leschinskaya A, Toomadj F, et al. Membrane characterization and solute diffusion in porous composite nanocellulose membranes for hemodialysis. Cellulose, 2013, 20: 2959–2970
14 Quinlan P J, Tanvir A, Tam K C. Application of the central composite design to study the flocculation of an anionic azo dye using quaternized cellulose nanofibrils. Carbohydr Polym, 2015, 133: 80–89
15 Yu H Y, Zhang D Z, Lu F F, et al. New approach for single-step extraction of carboxylated cellulose nanocrystals for their use as adsorbents and flocculants. ACS Sust Chem Eng, 2016, 4: 2632–2643
16 Carpenter A W, de Lannoy C F, Wiesner M R. Cellulose nanomaterials in water treatment technologies. Environ Sci Technol, 2015, 49: 5277–5287
17 Quellmalz A, Mihranyan A. Citric acid cross-linked nanocellulose-based paper for size-exclusion nanofiltration. ACS Biomater Sci Eng, 2015, 1: 271–276
18 Tang Z, Qiu C, McCutcheon J R, et al. Design and fabrication of electrospun polyethersulfone nanofibrous scaffold for high-flux nanofiltration membranes. J Polym Sci B Polym Phys, 2009, 47: 2288–2300
19 Mautner A, Lee K Y, Lahtinen P, et al. Nanopapers for organic solvent nanofiltration. Chem Commun, 2014, 50: 5778–5781
20 Sun D, Yang J, Wang X. Bacterial cellulose/TiO_2 hybrid nanofibers prepared by the surface hydrolysis method with molecular precision. Nanoscale, 2010, 2: 287–292
21 Huang W, Wang Y, Chen C, et al. Fabrication of flexible self-standing all-cellulose nanofibrous composite membranes for virus removal. Carbohydr Polym, 2016, 143: 9–17
22 Sato A, Wang R, Ma H, et al. Novel nanofibrous scaffolds for water filtration with bacteria and virus removal capability. J Electron Microsc, 2011, 60: 201–209
23 Sharma P R, Chattopadhyay A, Sharma S K, et al. Nanocellulose from spinifex as an effective adsorbent to remove cadmium(II) from water. ACS Sustain Chem Eng, 2018, 6: 3279–3290
24 Wu C, Wang Y, Gao B, et al. Coagulation performance and floc characteristics of aluminum sulfate using sodium alginate as coagulant aid for synthetic dying wastewater treatment. Separation Purification Tech, 2012, 95: 180–187
25 Suopajärvi T, Liimatainen H, Hormi O, et al. Coagulation-flocculation treatment of municipal wastewater based on anionized nanocelluloses. Chem Eng J, 2013, 231: 59–67
26 Feng X, Huang R Y M. Liquid separation by membrane pervaporation: A review. Indust Eng Chem Res, 1997, 36: 1048–1066
27 Werber J R, Osuji C O, Elimelech M. Materials for next-generation desalination and water purification membranes. Nat Rev Mater, 2016, 1: 16018
28 He X, Male K B, Nesterenko P N, et al. Adsorption and desorption of methylene blue on porous carbon monoliths and nanocrystalline cellulose. ACS Appl Mater Interfaces, 2013, 5: 8796–8804
29 Alsbaiee A, Smith B J, Xiao L, et al. Rapid removal of organic micropollutants from water by a porous β-cyclodextrin polymer. Nature, 2016, 529: 190–194
30 Korotta-Gamage S M, Sathasivan A. A review: Potential and challenges of biologically activated carbon to remove natural organic matter in drinking water purification process. Chemosphere, 2017, 167: 120–138
31 Mahmoudi K, Hamdi N, Srasra E. Study of adsorption of methylene blue onto activated carbon from lignite. Surf Engin Appl Electrochem, 2015, 51: 427–433
32 Wang B, Torres-Rendon J G, Yu J, et al. Aligned bioinspired cellulose nanocrystal-based nanocomposites with synergetic mechanical properties and improved hygromechanical performance. ACS Appl Mater Interfaces, 2015, 7: 4595–4607
33 Kardam A, Raj K R, Srivastava S, et al. Nanocellulose fibers for biosorption of cadmium, nickel, and lead ions from aqueous solution. Clean Techn Environ Policy, 2013, 16: 385–393
34 Zhang Z, Sèbe G, Rentsch D, et al. Ultralightweight and flexible silylated nanocellulose sponges for the selective removal of oil from water. Chem Mater, 2014, 26: 2659–2668
35 Metreveli G, Wågberg L, Emmoth E, et al. A size-exclusion nanocellulose filter paper for virus removal. Adv Healthcare Mater, 2014, 3: 1546–1550
36 Xie K, Zhao W, He X. Adsorption properties of nano-cellulose hybrid containing polyhedral oligomeric silsesquioxane and removal of reactive dyes from aqueous solution. Carbohydr Polym, 2011, 83: 1516–1520
37 Anirudhan T S, Deepa J R, Christa J. Nanocellulose/nanobentonite composite anchored with multi-carboxyl functional groups as an adsorbent for the effective removal of cobalt(II) from nuclear industry wastewater samples. J Colloid Interface Sci, 2016, 467: 307–320
38 Wen X, Zheng Y, Wu J, et al. Immobilization of collagen peptide on dialdehyde bacterial cellulose nanofibers via covalent bonds for tissue engineering and regeneration. Int J Nanomed, 2015, 4623–4637
39 Zhu H, Luo W, Ciesielski P N, et al. Wood-derived materials for green electronics, biological devices, and energy applications. Chem Rev, 2016, 116: 9305–9374
40 Sharma R, Alam F, Sharma A K, et al. ZnO anchored graphene hydrophobic nanocomposite-based bulk heterojunction solar cells showing enhanced short-circuit current. J Mater Chem C, 2014, 2: 8142–8151
41 Fang Z, Zhu H, Yuan Y, et al. Novel nanostructured paper with ultrahigh transparency and ultrahigh haze for solar cells. Nano Lett, 2014, 14: 765–773
42 Fukuzumi H, Fujisawa S, Saito T, et al. Selective permeation of hydrogen gas using cellulose nanofibril film. Biomacromolecules, 2013, 14: 1705–1709
43 Shah K J, Imae T. Selective gas capture ability of gas-adsorbent-incorporated cellulose nanofiber films. Biomacromolecules, 2016, 17: 1653–1661
44 Ghosh A K, Bandyopadhyay P. A simple strategy for charge selective biopolymer sensing. Chem Commun, 2011, 47: 8937–8939
45 Sharma P R, Varma A J. Functional nanoparticles obtained from cellulose: Engineering the shape and size of 6-carboxycellulose. Chem Commun, 2013, 49: 8818–8820
46 Reid M S, Villalobos M, Cranston E D. Benchmarking cellulose nanocrystals: From the laboratory to industrial production. Langmuir, 2017, 33: 1583–1598
47 Xu X, Liu F, Jiang L, et al. Cellulose nanocrystals vs. cellulose nanofibrils: A comparative study on their microstructures and effects as polymer reinforcing agents. ACS Appl Mater Interfaces, 2013, 5: 2999–3009
48 Saito T, Kimura S, Nishiyama Y, et al. Cellulose nanofibers prepared by TEMPO-mediated oxidation of native cellulose. Biomacromolecules, 2007, 8: 2485–2491
49 Isogai A, Saito T, Fukuzumi H. TEMPO-oxidized cellulose nanofibers. Nanoscale, 2011, 3: 71–85
50 Han J, Zhou C, French A D, et al. Characterization of cellulose II nanoparticles regenerated from 1-butyl-3-methylimidazolium chloride. Carbohydr Polym, 2013, 94: 773–781
51 Tzhayik O, Pulidindi I N, Gedanken A. Forming nanospherical cellulose containers. Ind Eng Chem Res, 2014, 53: 13871–13880
52 Sharma P R, Varma A J. Functionalized celluloses and their nanoparticles: Morphology, thermal properties, and solubility studies. Carbohydr Polym, 2014, 104: 135–142
53 Sharma P R, Kamble S, Sarkar D, et al. Shape and size engineered cellulosic nanomaterials as broad spectrum anti-microbial compounds.

Int J Biol Macromol, 2016, 87: 460–465
54 Sharma P R, Rajamohanan P R, Varma A J. Supramolecular transitions in native cellulose-I during progressive oxidation reaction leading to quasi-spherical nanoparticles of 6-carboxycellulose. Carbohydr Polym, 2014, 113: 615–623
55 Sharma P R, Joshi R, Sharma S K, et al. A simple approach to prepare carboxycellulose nanofibers from untreated biomass. Biomacromolecules, 2017, 18: 2333–2342
56 Nechyporchuk O, Belgacem M N, Pignon F. Current progress in rheology of cellulose nanofibril suspensions. Biomacromolecules, 2016, 17: 2311–2320
57 Luo G, Xie L, Zou Z, et al. Evaluation of pretreatment methods on mixed inoculum for both batch and continuous thermophilic biohydrogen production from cassava stillage. Bioresour Tech, 2010, 101: 959–964
58 Amiralian N, Annamalai P K, Memmott P, et al. Easily deconstructed, high aspect ratio cellulose nanofibres from Triodia pungens; an abundant grass of Australia's arid zone. RSC Adv, 2015, 5: 32124–32132
59 Su Y, Burger C, Ma H, et al. Morphological and property investigations of carboxylated cellulose nanofibers extracted from different biological species. Cellulose, 2015, 22: 3127–3135
60 Saito T, Nishiyama Y, Putaux J L, et al. Homogeneous suspensions of individualized microfibrils from TEMPO-catalyzed oxidation of native cellulose. Biomacromol, 2006, 7: 1687–1691
61 Puangsin B, Yang Q, Saito T, et al. Comparative characterization of TEMPO-oxidized cellulose nanofibril films prepared from non-wood resources. Int J Biol Macromol, 2013, 59: 208–213
62 Meng Q, Li H, Fu S, et al. The non-trivial role of native xylans on the preparation of TEMPO-oxidized cellulose nanofibrils. React Funct Poly, 2014, 85: 142–150
63 Su Y, Burger C, Ma H, et al. Exploring the nature of cellulose microfibrils. Biomacromolecules, 2015, 16: 1201–1209
64 Amiralian N, Annamalai P K, Memmott P, et al. Isolation of cellulose nanofibrils from Triodia pungens via different mechanical methods. Cellulose, 2015, 22: 2483–2498
65 Jacobsen S E, Wyman C E. Cellulose and hemicellulose hydrolysis models for application to current and novel pretreatment processes. Appl Biochem Biotechnol, 2000, 84-86: 81–96
66 Ma H, Burger C, Hsiao B S, et al. Ultra-fine cellulose nanofibers: New nano-scale materials for water purification. J Mater Chem, 2011, 21: 7507–7510
67 Okita Y, Saito T, Isogai A. Entire surface oxidation of various cellulose microfibrils by TEMPO-mediated oxidation. Biomacromolecules, 2010, 11: 1696–1700
68 Mao Y, Liu K, Zhan C, et al. Characterization of nanocellulose using small-angle neutron, X-ray, and dynamic light scattering techniques. J Phys Chem B, 2017, 121: 1340–1351
69 Sugiyama J, Vuong R, Chanzy H. Electron diffraction study on the two crystalline phases occurring in native cellulose from an algal cell wall. Macromolecules, 1991, 24: 4168–4175
70 Fujisaki Y, Koga H, Nakajima Y, et al. Transparent nanopaper-based flexible organic thin-film transistor array. Adv Funct Mater, 2014, 24: 1657–1663
71 Cosgrove D J. Growth of the plant cell wall. Nat Rev Mol Cell Bio, 2005, 6: 850–861
72 Kumar R, Hu F, Hubbell C A, et al. Comparison of laboratory delignification methods, their selectivity, and impacts on physiochemical characteristics of cellulosic biomass. Bioresour Tech, 2013, 130: 372–381
73 Okita Y, Saito T, Isogai A. TEMPO-mediated oxidation of softwood thermomechanical pulp. Holzforschung, 2009, 63: 529–535
74 Dimmel D R, Karim M R, Savidakis M C, et al. Pulping catalysts from lignin (5). Nitrogen dioxide oxidation of lignin models to benzoquinones. J Wood Chem Technol, 1996, 16: 169–189
75 Sharma P R, Zheng B, Sharma S K, et al. High aspect ratio carboxycellulose nanofibers prepared by nitro-oxidation method and their nanopaper properties. ACS Appl Nano Mater, 2018, 1: 3969–3980